

# Simple tunable phase-locked lasers for quantum technologies

NICOLA AGNEW<sup>1,\*</sup>, DAVID LOWIT<sup>1,\*</sup>, AND AIDAN S. ARNOLD<sup>1,†</sup>

<sup>1</sup>SUPA, Department of Physics, University of Strathclyde, Glasgow G4 0NG, United Kingdom.

\* These authors contributed equally.

† aidan.arnold@strath.ac.uk

Compiled April 26, 2024

**In a wide range of quantum technology applications, ranging from atomic clocks to the creation of ultracold or quantum degenerate samples for atom interferometry, optimal laser sources are critical. In particular, two phase-locked laser sources with a precise difference frequency are needed for efficient coherent population trapping (CPT) clocks, gray molasses laser cooling, or driving Raman transitions. Here we show how a simple cost-effective laser diode can selectively amplify only one sideband of a fiber-electrooptically-modulated seed laser to produce moderate-power phase-locked light with sub-Hz relative linewidth and tunable difference frequencies up to  $\approx 15$  GHz. The architecture is readily scalable to multiple phase-locked lasers and could conceivably be used for future on-chip compact phase-locked laser systems for quantum technologies.**

<http://dx.doi.org/10.1364/ao.XX.XXXXXX>

Quantum technology is burgeoning, and there are a wide variety of application areas requiring laser light with a frequency spectrum comprising exactly two modes that are phase-locked to each other – essentially frequency-offset laser ‘clones’ ideally with a delta-function frequency beat note. This paper demonstrates a simple  $> 100$  mW laser system fulfilling this criterion, relevant for applications in both thermal and ultracold CPT atomic clocks [1–5], Raman pulses for mirrors and beamsplitters in atom interferometry [6–10], as well as pulses relevant for logic gates in quantum computing with both atoms and ions [11–15], and Doppler-broadening thermometry [16, 17]. We foresee utility in all of these areas, however, here we focus on the specific moderate-power application of sub-Doppler laser cooling using the topical technique of gray molasses (GM) [18].

The first observations of sub-Doppler [19], and GM [18] cooling schemes now facilitate research into quantum degeneracy, communication, optics and computing as well as technology applications [20–26]. In particular GM cooling [27] has recently yielded striking phase-space density enhancements in several alkali metals including Li [28, 29], Na [30], K [31–33], Rb [34, 35], and Cs [18, 36] and it has also been employed in molecules [37], and grating magneto-optical traps [38].

Regardless of species, a crucial requirement for GM (and

many clocks and Raman pulses) is phase coherence between precisely two laser frequencies incident on the atoms [35]. Our laser system is capable of cost-effectively producing the requisite moderate-power dual-frequency phase-coherent light, with a widely tunable difference frequency. The system is also designed to be integrated into existing laser cooling systems.

Electro-optic modulators (EOMs [39, 40]) are ideal for making multi-frequency phase-coherent light, without independent laser systems. However, while free-space EOMs can handle higher optical input powers (Watts), they have low fractional sideband power – particularly for Rb and Cs, with their large ground state hyperfine splittings – with only 0.1% relative RF frequency tunability due to the necessary resonant RF drive circuit [41]. Conversely, fiber EOMs have extremely wide frequency tunability, and large fractional sidebands for low RF input power – but at wavelengths suitable for most alkali metal transitions they can only carry low optical powers ( $\approx 25$  mW) without damage, with  $\approx 4$  dB insertion loss [42].

A major disadvantage of both fiber and free-space EOMs is that any positive frequency sideband has an equal amplitude negative frequency sideband, in addition to the carrier. There are therefore always unwanted laser frequency sidebands – which in the best case are wasted laser power, and in the worst case cause resonant heating or lead to light shifts affecting the performance of e.g. atomic clocks. IQ modulators [43, 44], Serrodyne [45] and other alternative techniques [46, 47] offer the ability to make approximately single-sideband modulation, but without the cost-effectiveness, simplicity or flexibility we demonstrate here. We also suspect that our technique is likely to suppress EOM-induced residual amplitude modulation [48].

A key part of our phase-locked laser system (Fig. 1) is optical injection locking (OIL), whereby light from a seed laser (SL [49]) is injected into a temperature-stabilised amplifier laser (AL). By tuning the AL internal diode cavity using its current, the AL’s gain can be matched to the injected light frequency. The AL and SL can thereby synchronise frequencies and also phases. Importantly, unlike the broadband gain of a tapered amplifier, the AL current can be tuned to only amplify one narrow-band laser frequency and filter out all others. We can therefore selectively amplify only one fiber-EOM frequency sideband of our SL [50]. This allows cheap laser diodes to be used as frequency filtering phase-locked amplifiers without compromising on laser quality.

The current SL in our test setup is a Littman low-power

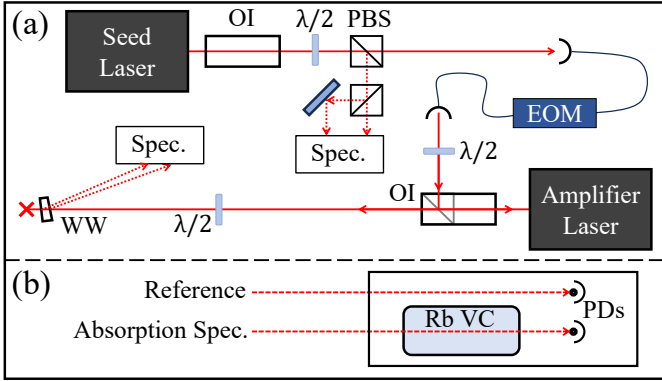


**Fig. 1.** Experimental diagram (a), with the seed and amplifier laser (SL, AL) low-intensity spectroscopy setup in (b). Abbreviations: optical isolator (OI), half-wave plate ( $\lambda/2$ ), fiber electro-optic modulator (EOM), polarising beamsplitter (PBS), wedged window (WW), photodiode (PD), and vapor cell (VC).

780.24 nm commercial external cavity diode laser (ECDL [51]) with a 100 GHz mode-hop-free frequency scan, although a Littrow ECDL [52] or other laser type [53–59] could also be used. A small portion of the SL beam was used for low-intensity ( $< 1 \mu\text{W}/\text{cm}^2$  [60]) spectroscopy [61], Fig. 1 (a,b), through a 74 mm Rb vapour cell. The transmission signal is normalised by dividing with the intensity of a reference beam [17]. Narrow-band frequency filtering with a 1.2 nm FWHM filter gave a 50-fold reduction to SL amplified spontaneous emission [17].

SL light not used in spectroscopy was coupled into the single-mode, polarisation-maintaining fibre EOM, and its output (injection beam) was then aligned into the AL cavity via the rejection output port of an optical isolator [62]. To quantify injection locking performance the AL output was measured in its own low-intensity spectroscopy setup. This enables simple characterisation of the SL vs. AL output using Doppler-broadened dips of the  $D_2$  line of the natural isotopes of Rb (Fig. 2(a)).

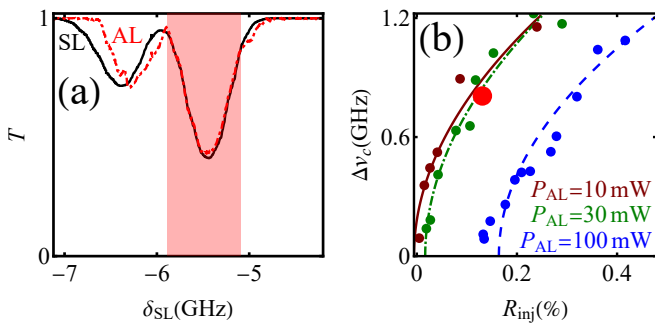


**Fig. 2.** (a) The SL (black) and AL (red, dot-dashed) low-intensity transmission ( $T$ ) spectroscopy signals in a scan of SL detuning ( $\delta_{\text{SL}}$ ) over the two  $F = 2 \leftrightarrow F'$  and  $F = 3 \leftrightarrow F'$  Doppler-broadened  $^{87}\text{Rb}$  and  $^{85}\text{Rb}$   $D_2$  lines, respectively. The highlighted large data point in (b) illustrates our empirical method to extract  $\Delta\nu_c$  from the region where the AL faithfully copies the SL (red shaded region) (b) Capture range  $\Delta\nu_c$  as a function of injection ratio  $R_{\text{inj}}$  for three AL powers  $P_{\text{AL}} = (10, 30, 100)$  mW (red, green, blue). The corresponding Eq. 1 squareroot fits (solid, dash-dotted and dashed) assume a 50 GHz FSR, and allow for an  $R_{\text{th}}$  offset.

Correct SL beam alignment into the AL cavity can be optimised by maximising the observed capture range, with Fig. 2(a) corresponding to SL input and AL output powers of  $13 \mu\text{W}$  and  $10 \text{ mW}$ , respectively, when using no EOM sidebands. We note the SL beam is fibered and circular, whereas the AL beam profile is elliptical, indicating that better AL-SL mode-matching will enhance injection performance.

A measurable parameter and performance metric for OIL is the capture range ( $\Delta\nu_c$ ) which describes the frequency range over which the AL copies the injected light. For a diode laser, this is given by [63]:

$$\Delta\nu_c = \text{FSR} \sqrt{(1 + \alpha^2)(R_{\text{inj}} - R_{\text{th}})}, \quad (1)$$

where FSR is the free spectral range of the AL diode cavity (typically  $\approx 50$  GHz),  $\alpha$  is the linewidth enhancement factor [64], and  $R_{\text{inj}} = P_{\text{inj}}/P_{\text{AL}}$  is the ratio of the injected beam power to the AL power. We illustrate this equation experimentally in Fig. 2(b), with better agreement found using a threshold injection  $R_{\text{th}}$  ratio that increases with  $P_{\text{AL}}$  [65].

We now consider the AL behaviour when the fiber EOM is activated, with modulation frequency  $\Delta\nu_m = 6.8$  GHz (Fig. 3). The EOM beam's optical power is mainly distributed across the  $0^{\text{th}}$  (carrier) and  $\pm 1^{\text{st}}$  (sideband) EOM orders, with relative amplitudes determined by the input RF power and frequency [66]. Injection locking the AL to an individual sideband, with less laser power, therefore slightly reduces the capture range. Despite the lower overall injection power in the carrier and two first-order sidebands, Fig. 3(a) shows successful injection locking of the AL to the carrier, or either first-order sideband. When the SL detuning is ( $-13.66$ ,  $-6.83$ , and  $0$ ) GHz then the relative detuning of the AL to the SL is ( $6.83$ ,  $0$ , and  $-6.83$ ) GHz (i.e. the AL detuning is always  $\sim -6.83$  GHz, and the  $+1^{\text{st}}$ ,  $0^{\text{th}}$ , and  $-1^{\text{st}}$  EOM sidebands are amplified as the SL detuning increases).

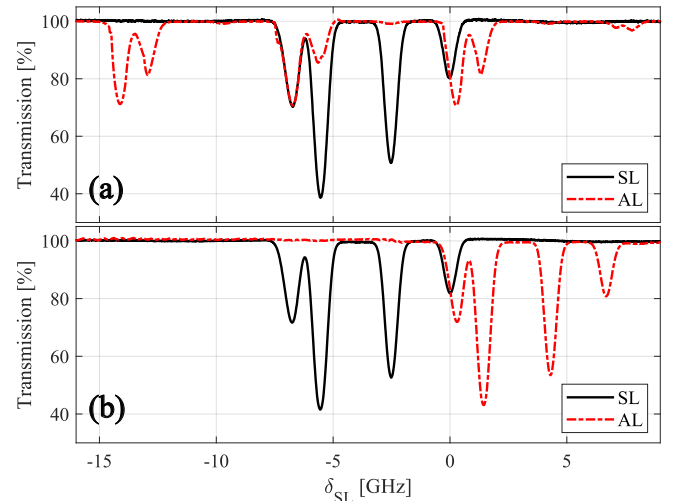


**Fig. 3.** (a) Optical injection locking of the AL with multi-frequency injection light at  $\Delta\nu_m = 6.83$  GHz ( $R_{\text{inj}} = 0.5\%$  with  $P_{\text{AL}} = 81.0$  mW and  $P_{\text{inj}} = 0.390$  mW). The AL current is constant and adjusted to only copy the frequency of the  $^{87}\text{Rb}$   $F = 2 \leftrightarrow F'$  transitions, for different EOM sidebands, as the SL frequency increases. (b) By using a linear ramp of the AL current, synchronised to the SL frequency scan, the capture range for only the  $-1^{\text{st}}$  EOM sideband is widened.

Applying a linear ramp of the AL current, synchronised to the SL frequency scan, extends the AL's  $-1^{\text{st}}$  order single-sideband EOM capture range significantly (Fig. 3(b)) [67]. By changing the AL current one can instead extend the scan range of the  $0^{\text{th}}$  or  $+1^{\text{st}}$  EOM sideband. We note that the behaviour shown in Fig. 3 extends fairly well to modulation frequencies up to  $\Delta\nu_m = 15$  GHz. The lower modulation frequency bound is complicated when the regions of incomplete AL frequency cloning of the SL seen in Fig. 3 overlap for different EOM sidebands, but modulation frequencies  $< 3$  GHz can still be realised.

While the low-intensity spectroscopy method presented here shows that the AL is a good frequency-offset copy of the SL, it does not in itself prove phase-locking. We therefore also performed an RF beat note measurement, by combining mode-matched co-polarised AL and SL beams on a (0 – 25) GHz photodiode [68]. The SL beam used for the beatnote was unmodulated by the EOM, but frequency offset by -80 MHz using an acousto-optic modulator. The resulting beat-note (Fig. 4) has a 1 Hz full width half maximum linewidth over a 10 Hz span – at the frequency resolution limit of the RF spectrum analyser used for the measurement. Moreover, the -80 MHz SL offset allowed us to use the distinct beatnotes to separate and accurately determine the relative amplitudes of any unwanted EOM orders from the AL. We observed a typical AL EOM sideband rejection ratio of  $\approx 20$  dB under the conditions of Fig. 4.

By explicitly considering the laser sources required for GM cooling of rubidium, we explore a specific application note. Existing GM cooling studies in  $^{85}\text{Rb}$  and  $^{87}\text{Rb}$  report using laser powers of order 100 mW [34, 35]. Although stable OIL with a small capture range has been demonstrated in diode lasers with low injection ratios  $\approx 10^{-5}$  [49], it is beneficial to have a higher injection power as a larger capture range provides reduced intensity noise in the AL [69]. To achieve 100 mW powers over the 0.5 GHz capture range needed for Rb gray molasses, sideband injection powers  $< 1$  mW suffice (Fig. 2(a)).

To most easily obtain the two laser frequencies for the MOT, normal molasses and gray molasses, a  $\approx 100$  mW repump laser can be locked to the  $F = I - 1/2 \leftrightarrow F' = I + 1/2$  transition, and

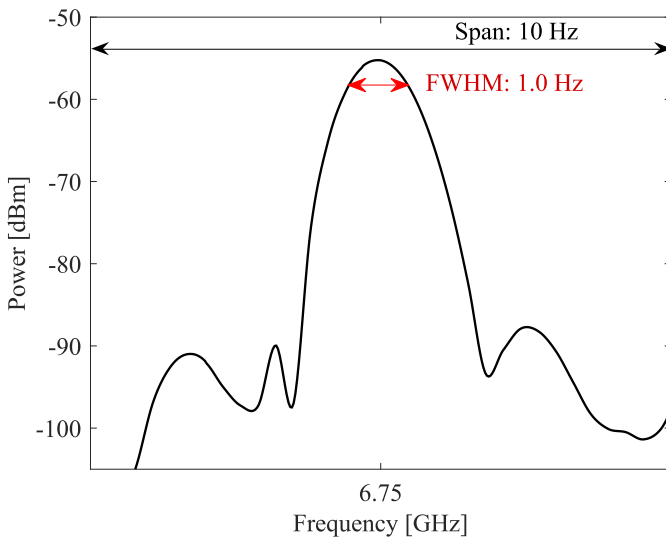


**Fig. 4.** Radio frequency beatnote centred at 6.75 GHz between the AL-amplified  $-1^{\text{st}}$  order EOM sideband (phase-modulated at 6.83 GHz) and the -0.08 GHz-offset SL laser. The span is set to the minimum value of the RF spectrum analyser.

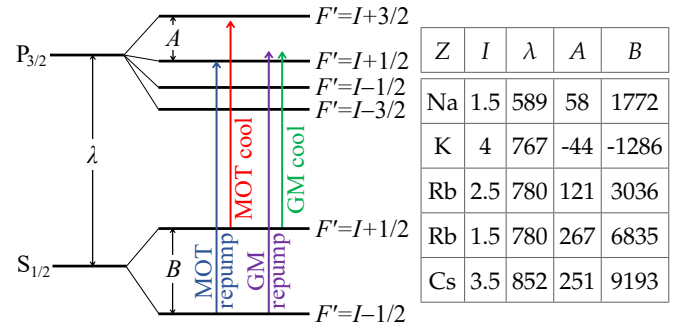


**Fig. 5.** The  $D_2$ -line hyperfine manifold with MOT and GM transitions for the appropriate alkali metal isotopes  $^{23}\text{Na}$ ,  $^{40}\text{K}$ ,  $^{85}\text{Rb}$ ,  $^{87}\text{Rb}$  and  $^{133}\text{Cs}$ . The nuclear spin is  $I$ , the wavelength is  $\lambda$  in nm, and  $A$  and  $B$  are hyperfine level splittings in MHz.

a small portion of modulated light from this SL creates an AL that can be red-detuned from approximately  $B - A$  to  $B$  (Fig. 5), using the EOM modulation frequency. To be specific, for  $^{87}\text{Rb}$  the  $D_2$  SL laser needs a sub-Doppler lock to the  $F = 1 \leftrightarrow F' = 2$  transition (e.g. using hyperfine pumping spectroscopy [70]), and we wish the AL to amplify only the red sideband of the fiber EOM in the range of 6.58 to 6.83 GHz. This produces a phase-locked cooling transition beam which can be combined with the repump beam for all stages of cooling.

For GM using the  $D_2$  atomic line, e.g.  $^{40}\text{K}$  [32],  $^{87}\text{Rb}$  [35] and Cs [36] (but diodes don't currently exist for Na [30]), our laser system tunability means that the *same*  $D_2$  laser system can be used for regular magneto-optical trapping and optical molasses, prior to GM cooling, obviating the need for an additional GM laser system which is sometimes used [18]. While applications are not limited to this species, our  $D_2$  line laser system is tested with GM cooling of Rb in mind. For parameters relevant for other alkali metal species see the general level diagram and table in Fig. 5.

In conclusion, we have developed a simple, high-power, relative-frequency-tunable phase-locked two-laser system that is ideal for magneto-optical trapping, optical molasses and gray molasses using the same  $D_2$  setup. Moreover, the design can also be useful in clock, interferometry, quantum computing and alkali metal Doppler thermometry [16, 17] experiments. The architecture could also conceivably be used for future on-chip compact phase-locked laser systems for quantum technologies [71]. The phase-locking quality could be characterised further using the approach in [50], and the system could be improved in future by achieving better mode-matching between the SL and AL beam shapes, and using a higher-power AL laser diode [72]. For higher Watt-level powers a tapered amplifier could be used on the AL, after the AL diode removes unwanted EOM sidebands.

**Funding.** Engineering and Physical Sciences Research Council EP/T001046/1; National Physical Laboratory iCASE studentship EP/X525017/1.

**Acknowledgments.** We thank the wider EQOP quantum technology team for general support. Special thanks to Jon Pritchard and Erling Riis for proof-reading and improving the manuscript, and Graham Machin, Paul Griffin and Sonja Franke-Arnold for valuable discussions. For the purpose of open access, the authors have applied a Creative Commons Attribution (CC BY) licence to any Author Accepted Manuscript (AAM) version arising from this submission.

**Disclosures.** The authors declare no conflicts of interest.

**Data availability.** Data underlying the results presented in this paper are available in Ref. [TBD].

## REFERENCES

1. S. Knappe, V. Shah, P. D. D. Schwindt, *et al.*, *Appl. Phys. Lett.* **85**, 1460 (2004).
2. M. A. Hafiz, G. Coget, P. Yun, *et al.*, *J. Appl. Phys.* **121**, 104903 (2017).
3. X. Liu, E. Ivanov, V. I. Yudin, *et al.*, *Phys. Rev. Appl.* **8**, 054001 (2017).
4. J. D. Elgin, T. P. Heavner, J. Kitching, *et al.*, *Appl. Phys. Lett.* **115**, 033503 (2019).
5. R. Elvin, G. W. Hoth, M. Wright, *et al.*, *Opt. Express* **27**, 38359 (2019).
6. S. M. Dickerson, J. M. Hogan, A. Sugarbaker, *et al.*, *Phys. Rev. Lett.* **111** (2013).
7. A. V. Rakholia, H. J. McGuinness, and G. W. Biedermann, *Phys. Rev. Appl.* **2** (2014).
8. X. Wu, F. Zi, J. Dudley, *et al.*, *Optica* **4**, 1545 (2017).
9. L. Morel, Z. Yao, P. Cladé, and S. Guellati-Khélifa, *Nature* **588**, 61 (2020).
10. S. Abend, B. Allard, A. S. Arnold, *et al.*, *AVS Quantum Sci.* **5** (2023).
11. R. Blatt and C. F. Roos, *Nat. Phys.* **8**, 277 (2012).
12. K. McDonnell, L. Keary, and J. Pritchard, *Phys. Rev. Lett.* **129** (2022).
13. T. M. Graham, Y. Song, J. Scott, *et al.*, *Nature* **604**, 457 (2022).
14. S. J. Evered, D. Bluvstein, M. Kalinowski, *et al.*, *Nature* **622**, 268 (2023).
15. G. Bornet, G. Emperauger, C. Chen, *et al.*, *Nature* **621**, 728 (2023).
16. G.-W. Truong, E. F. May, T. M. Stace, and A. N. Luiten, *Phys. Rev. A* **83**, 033805 (2011).
17. N. Agnew, G. Machin, E. Riis, and A. S. Arnold, arxiv:2307.06229 (2023).
18. D. Boiron, C. Triché, D. R. Meacher, *et al.*, *Phys. Rev. A* **52**, R3425 (1995).
19. P. D. Lett, R. N. Watts, C. I. Westbrook, *et al.*, *Phys. Rev. Lett.* **61**, 169 (1988).
20. M. H. Anderson, J. R. Ensher, M. R. Matthews, *et al.*, *Science* **269**, 198 (1995).
21. W. Ketterle, *Rev. Mod. Phys.* **74**, 1131 (2002).
22. C. Foot, *Magnetic trapping, evaporative cooling and Bose-Einstein condensation* (Oxford University Press Inc., 2005), p. 224–229.
23. H. Perrin, P. Lemonde, F. Pereira dos Santos, *et al.*, *Comptes Rendus Physique* **12**, 417 (2011).
24. I. Bloch, J. Dalibard, and W. Zwerger, *Rev. Mod. Phys.* **80**, 885 (2008).
25. J. Dunningham, K. Burnett, and W. D. Phillips, *Philos. Trans. Royal Soc. A: Math. Phys. Eng. Sci.* **363**, 2165 (2005).
26. Z. Shi, Z. Li, P. Wang, *et al.*, *J. Opt. Soc. Am. B* **38**, 1229 (2021).
27. L. Gabardos, S. Lepoutre, O. Gorceix, *et al.*, *Phys. Rev. A* **99**, 023607 (2019).
28. A. Burchianti, G. Valtolina, J. A. Seman, *et al.*, *Phys. Rev. A* **90**, 043408 (2014).
29. A. T. Grier, I. Ferrier-Barbut, B. S. Rem, *et al.*, *Phys. Rev. A* **87**, 063411 (2013).
30. Z. Shi, Z. Li, P. Wang, *et al.*, *Chin. Phys. Lett.* **35**, 123701 (2018).
31. J. Ang'ong'a, C. Huang, J. P. Covey, and B. Gadway, *Phys. Rev. Res.* **4**, 013240 (2022).
32. G. D. Bruce, E. Haller, B. Peaudecerf, *et al.*, *J. Phys. B: At. Mol. Opt. Phys.* **50**, 095002 (2017).
33. D. R. Fernandes, F. Sievers, N. Kretschmar, *et al.*, *Europhys. Lett.* **100**, 63001 (2012).
34. C. Huang, S. Chai, and S.-Y. Lan, *Phys. Rev. A* **103**, 013305 (2021).
35. S. Rosi, A. Burchianti, S. Conclave, *et al.*, *Sci. Reports* **8** (2018).
36. Y.-F. Hsiao, Y.-J. Lin, and Y.-C. Chen, *Phys. Rev. A* **98**, 033419 (2018).
37. S. Truppe, H. J. Williams, M. Hambach, *et al.*, *Nat. Phys.* **2017** 13:12 **13**, 1173 (2017).
38. D. S. Barker, E. B. Norrgard, N. N. Klimov, *et al.*, *Opt. Express* **30**, 9959 (2022).
39. T. Kawanishi, T. Sakamoto, and M. Izutsu, *IEEE J. Sel. Top. Quantum Electron.* **13**, 79 (2007).
40. T. Kawanishi, *Electro-optic Modulation for Photonic Networks* (Springer Nature Switzerland, 2022).
41. Based on legacy Newport EOMs.
42. IXblue NIR-MPX800-LN-10-00-P-P-FA-FA.
43. X. Li, L. Deng, X. Chen, *et al.*, *Opt. Express* **25**, 9333 (2017).
44. L. Zhu, Y.-H. Lien, A. Hinton, *et al.*, *Opt. Express* **26**, 6542 (2018).
45. D. M. S. Johnson, J. M. Hogan, S. w. Chiow, and M. A. Kasevich, *Opt. Lett.* **35**, 745 (2010).
46. C. D. Macrae, K. Bongs, and M. Holynski, *Opt. Lett.* **46**, 1257 (2021).
47. U. Dammalapati, R. Elvin, P. F. Griffin and E. Riis, in preparation.
48. J. Gillot, S. Falzon Tetsing-Talla, S. Denis, *et al.*, *Opt. Express* **30**, 35179 (2022).
49. R. Kakarla, J. Schröder, and P. A. Andrekson, *Opt. Lett.* **43**, 5769 (2018).
50. M. J. Snadden, R. B. M. Clarke, and E. Riis, *Opt. Lett.* **22**, 892 (1997).
51. A 5 mW New Focus Vortex laser from the year 2000, with the same diode.
52. A. S. Arnold, J. S. Wilson, and M. G. Boshier, *Rev. Sci. Instruments* **69**, 1236–1239 (1998).
53. X. Baillard, A. Gauguet, S. Bize, *et al.*, *Opt. Commun.* **266**, 609–613 (2006).
54. S. S. Sané, S. Bennetts, J. E. Debs, *et al.*, *Opt. Express* **20**, 8915 (2012).
55. J. M. Pino, B. Luey, S. Bickman, and M. H. Anderson, “Miniature, compact laser system for ultracold atom sensors,” in *Photonic Applications for Aerospace, Commercial, and Harsh Environments IV*, A. A. Kazemi, B. C. Kress, and S. Thibault, eds. (SPIE, 2013).
56. P. H. Moriya, Y. Singh, K. Bongs, and J. E. Hastie, *Opt. Express* **28**, 15943 (2020).
57. E. Di Gaetano, S. Watson, E. McBrearty, *et al.*, *Opt. Lett.* **45**, 3529 (2020).
58. Y. Wang, J. A. Holguín-Lerma, M. Vezzoli, *et al.*, *Nat. Photonics* **17**, 338–345 (2023).
59. A. Isichenko, N. Chauhan, K. Liu, *et al.*, arxiv:2307.04947 (2023).
60. P. Siddons, C. S. Adams, C. Ge, and I. G. Hughes, *J. Phys. B: At. Mol. Opt. Phys.* **41**, 155004 (2008).
61. D. Pizzey, J. D. Briscoe, F. D. Logue, *et al.*, *New J. Phys.* **24**, 125001 (2022).
62. Similar performance and easier alignment are achieved by directly injecting the AL through the isolator, and extracting the AL beam through the isolator rejection port.
63. F. Mogensen, H. Olesen, and G. Jacobsen, *IEEE J. Quantum Electron.* **21**, 784 (1985).
64. The  $1 + \alpha^2$  ‘enhancement’ values in Fig. 2 are 0.23, 0.25 and 0.19, respectively, unlike the expected  $\geq 1$  values. We suspect this is because we are defining the capture range quite stringently – with a  $\sim 100\%$  fidelity rather than a 50% full-width-half-maximum range.
65. Surprisingly, this can’t be explained away by an imperfect diode facet anti-reflection coating, which would not change  $R_{th}$  with  $P_{AL}$ .
66. At 6.8 GHz with 20 dBm from an unamplified Windfreak SynthHD source we see a modulation depth around 0.4.
67. We used an inverting amplifier based on an op-amp, with optimised variable gain.
68. Thorlabs DXM25CF.
69. Z. Liu and R. Slavík, *J. Light. Technol.* **38**, 43 (2020).
70. D. A. Smith and I. G. Hughes, *Am. J. Phys.* **72**, 631–637 (2004).
71. J. P. McGilligan, K. Gallacher, P. F. Griffin, *et al.*, *Rev. Sci. Instruments* **93** (2022).
72. A. Daffurn, R. F. Offer, and A. S. Arnold, *Appl. Opt.* **60**, 5832 (2021).